Substorm Activity as a Driver of Energetic Pulsating Aurora

R. N. Troyer [1], A. N. Jaynes [1], S. L. Jones [2], S. R. Kaeppler [3], R. H. Varney [4], A. S. Reimer [4]

[1]Department of Physics and Astronomy, University of Iowa
[2]Formerly of NASA Goddard Space Flight Center
[3]Clemson University
[4]SRI International

Key Points:

- We analyzed the inverted energies for 53 pulsating aurora events and found a close relationship to substorms and AE index.
- The average total energy flux and spectral hardness increase closer to substorm onset and for higher AE indices.
- The spectral hardness remains enhanced for approximately 1 hour after substorm onset.

Corresponding author: Riley Troyer, `riley-troyer@uiowa.edu`

Abstract

Pulsating aurora are common diffuse-like aurora. Studies have suggested that their energy is higher than other types and possibly linked to substorm activity. There has yet to be a quantitative statistical study of pulsating aurora energy content. We analyzed the inverted energies from 53 events using the Poker Flat Incoherent Scatter Radar. We compared this to magnetic local time (MLT), AE index, and temporal proximity to substorm onset. There was a slight trend in MLT, but a much stronger one in relation to both temporal substorm proximity and AE index. For higher AE and closer temporal proximity the total energy flux and flux above 30 keV increased. In addition, this higher energy remained enhanced for an hour after substorm onset. Our results confirm the high energy nature of pulsating aurora, demonstrate the connection to substorms, and imply their importance to coupling between the magnetosphere and atmosphere.

Plain Language Summary

Not all aurora (northern lights) are bright and defined curtains of light. Diffuse aurora are more modest. Barely visible to the naked eye, they spread across large portions of the night sky and can be easily overlooked. Pulsating aurora are a common and more playful type of diffuse aurora. In one of these displays, widely varying patches of aurora blink on and off with with periods ranging up to 20 seconds. While they aren't as bright, it has been suspected that the electrons which cause pulsating aurora are much more energetic than other types of aurora. Since energetic electrons move faster and thus can reach further into the atmosphere, it is possible that pulsating aurora may affect terrestrial climate. To study this, we first need a better understanding of pulsating aurora energies and how they can vary. In this study, we looked at the energy of 55 pulsating aurora events. In doing so, we confirmed that the energy of pulsating aurora is much higher than other types of aurora. We also found that the most energetic aurora happen close in time to a magnetic disturbance known as a substorm and that a stronger disturbance leads to higher energies.

1 Introduction

Pulsating aurora are a stark contrast to the bright curtains of discrete aurora that often precede them. Diffuse and barely visible to the naked eye, this type of aurora is

most often observed a few hours after magnetic midnight (e.g., Oguti et al., 1981; Jones et al., 2011). Often staying out for hours, pulsating aurora can cover large portions of the sky and in some cases expand over entire sections of the auroral region (Jones et al., 2013). Using SuperDarn and imager data, E. Bland et al. (2021) found that around half of pulsating aurora events extend between 4-5 hours of magnetic local time and between 62° to 70° in magnetic latitude. Over this area, auroral patches blink on and off with periods ranging up to around 20 seconds (e.g., Davis, 1978; Lessard, 2012). Adding to the show, individual patches can be remarkably varied with differing periods, shapes, and sizes typically between 10s to 100s of kilometers (Johnstone, 1978; Lessard, 2012). Figure 1 panels A1-A3 shows a typical example of pulsating aurora that occurred on October 13, 2016 over the Poker Flat Research Range. The red oval highlights a patch that turns on and off during the three images.

Some studies have attempted to classify different types of pulsating aurora. For instance, Royrvik and Davis (1977) classified events into patches, arcs, and arc segments. More recently, Grono and Donovan (2018) made a distinction between the quickly varying amorphous pulsating aurora, more regular patchy pulsating aurora, and non-pulsating patchy aurora. We included all of these when making a general identification of pulsating aurora.

Numerous studies have shown that the electrons responsible for pulsating aurora originate in the equatorial region of the outer Van Allen radiation belt. These electrons are pitch-angle scattered into the upper-atmosphere through wave-particle interactions, most likely with lower-band chorus waves (Nishimura et al., 2010, 2011; Jaynes et al., 2013; Kasahara et al., 2018; Hosokawa et al., 2020). Previous studies have found that the energy of these particles is substantially higher than other auroral types, ranging between 10s to 100s of keV (e.g., Whalen et al., 1971; Sandahl et al., 1980). This energy can vary substantially, even within individual events. Jones et al. (2009) notes often seeing a decrease in energy throughout an event. Hosokawa and Ogawa (2015) found, using the European Incoherent Scatter Radar, that the energy spectrum of pulsating aurora is harder when a patch is “on” versus when it is “off” with only background aurora present.

Several papers concerning the height of pulsating aurora indicate that there may also be some relation between energy and substorm onset. In the two events that they

analyzed, Oyama et al. (2017) found that the atmospheric electron densities associated with pulsating aurora dropped to a lower altitude following a substorm. This would indicate an influx of higher energy electrons capable of penetrating further into the atmosphere. These results match up with the statistical study of Hosokawa and Ogawa (2015) who showed that the electron density profile of pulsating aurora extends lower in altitude during periods with a large AE index (> 500). This previous work is a strong indicator of the increase in higher energy electrons, or spectral hardening, during geomagnetically perturbed conditions. However, the results are qualitative as altitude is only a proxy for energy. Wing et al. (2013) did conduct a statistical study of auroral energies associated with substorm onset. They made distinctions between broadband (Alfvén accelerated) electrons, monoenergetic (parallel electric field accelerated) electrons, and diffuse (whistler mode wave scattered) electrons. They found that energies increase in association to substorms for all types, with the largest for diffuse electrons. However, they made no distinction between general diffuse and pulsating aurora.

These previous investigations make a strong case for a link between substorm activity and the energy of pulsating aurora. More energetic events seem to occur right after substorm onset. However, direct evidence supporting this hypothesis has yet to be established. In this paper, we provide statistical evidence, using inverted differential energy fluxes, that substorm activity is indeed correlated with higher energies in pulsating aurora. The results shown here both confirm the high-energy nature of pulsating aurora and specify the correlation between pulsating aurora energy and substorms.

2 Data

This paper presents a data set of 57 pulsating aurora events between 2012 and 2021, four of which (2015-01-13, 2017-08-17, 2018-12-30, and 2021-01-13) were not usable for our energy inversion. This data was captured over 51 days with the Poker Flat Research Range All Sky Imager (PFRR ASI). A table of these days can be found in the supplemental material. This instrument takes an image approximately every 12 seconds at 428 nm, 557 nm, and 630 nm. We used the 428 nm images because they have a direct correlation with total energy flux (Kasting & Hays, 1977). Therefore, we expect pulsating aurora, which are associated with higher energies, to stand out in this wavelength. It is worth noting that despite the 12 second period of the camera, we can still accurately identify pulsating aurora, see Figure 1 panels A1-A3.

For each of these pulsating aurora events, the Poker Flat Incoherent Scatter Radar (PFISR) was running one of the D-region modes (MSWinds23, MSWinds26, or MSWinds27) (Kaeppler et al., 2020). These modes all use 13-baud Barker codes with 10 μs baud, oversampled at 5 mus (0.75 km range resolution) to provide electron density as function of range and time over ranges between 40 to 144 km. This study uses one minute integration times, which means the electron density profiles are averaged over many cycles of the pulsating aurora. These modes all use four beam directions (magnetic zenith, vertical, north-west, and north-east). This study uses the vertical beam data since it is systematically more sensitive than the magnetic zenith direction at PFISR. The magnetic zenith is close to the phased-array antenna grating lobe steering limit. Furthermore, the MSWinds27 modes revisit the beams unevenly such that the vertical beam receives 16 times more pulses than the other beams, resulting in a factor of 4 improvement in the statistical uncertainty relative to the other beams. The vertical beam is only $< 20^\circ$ away from the magnetic zenith direction which is sufficiently small for our inversions to neglect any variations across magnetic field lines. Supplementary Appendix 2 gives additional information on the PFISR experiments and data processing. Figure 1 panel B shows an example of electron densities measured by PFISR MSWinds23 during a period of typical pulsating aurora on October 13, 2016. This event began just after a substorm and continued until the end of the PFISR experiment. This event is an excellent example of the electron density profile pushing to lower altitudes during pulsating aurora.

3 Analysis

In this study, we quantify the differential energy flux of pulsating aurora, in particular, the higher energy portion. Previous investigations have indicated that the energy of pulsating aurora varies significantly both within and between events, often associated with substorm activity (Jones et al., 2009; Wing et al., 2013; Hosokawa & Ogawa, 2015). Based on these results, we chose to examine variations related to magnetic local time (MLT), AE index, and an epoch associated with temporal substorm proximity. We set an epoch time of 0 to substorm onsets taken from lists created by Newell and Gjerloev (2011), Forsyth et al. (2015), and Ohtani and Gjerloev (2020). We chose these three lists because they cover a time period that encompasses our data. Each method identifies substorms in a slightly different way, so by including all three we can identify more events over a broader range of criteria. We limited these substorms to those that occurred

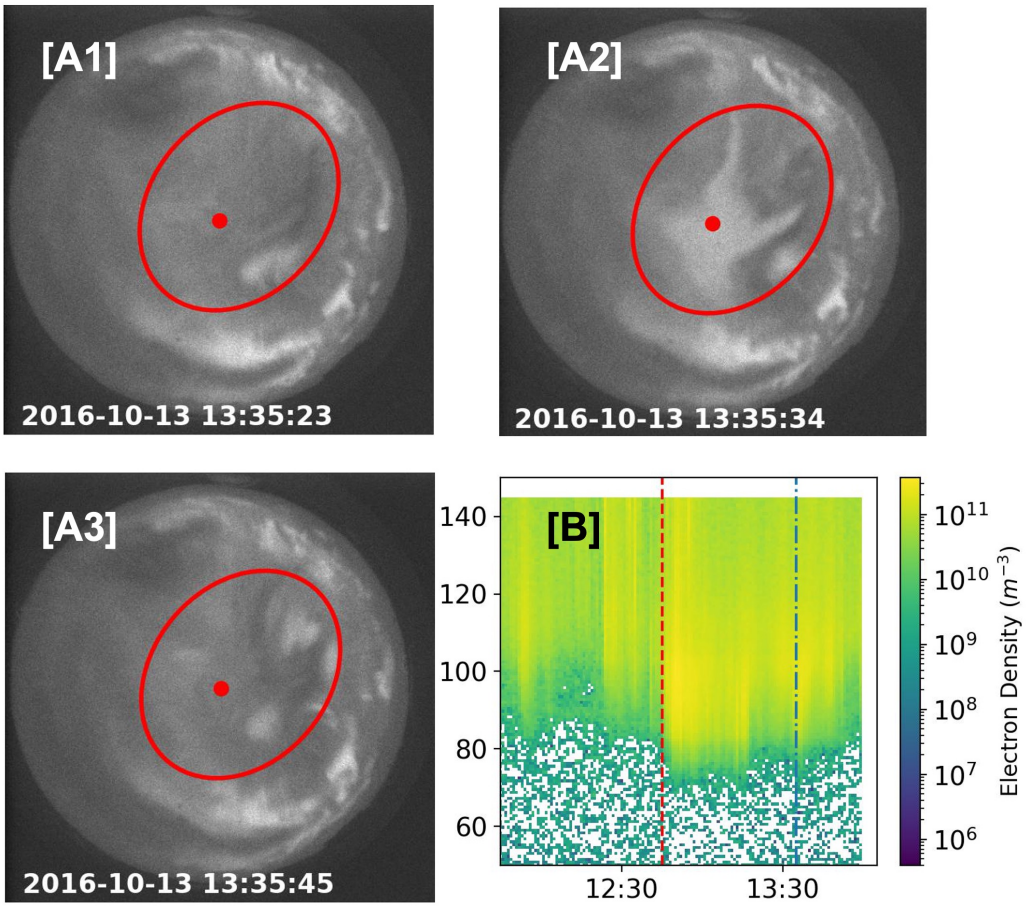

Figure 1. Panels A1-A3 show a series of 428 nm images from the Poker Flat Research Range All Sky Imager with several pulsating aurora patches of differing sizes. Even though the imaging rate is 12 seconds, we can still identify pulsating aurora. The red dot indicates the center of each image and thus the approximate location of the vertical PFISR beam. Panel B is the PFISR electron number density data for a pulsating aurora event on October 13, 2016. The data is plotted vs. altitude in km and universal time. The dashed red line indicates the start of pulsating aurora. The dashed and dotted blue line indicates when the images were taken. The radar stopped taking data before the pulsating aurora ended.

within $\pm 15^\circ$ longitude and $\pm 8^\circ$ latitude of the Poker Flat Research Range. For the AE indices, we used archived 10-minute predicted values (Luo et al., 2013).

As a proxy for energy, we chose the lower altitude boundary that PFISR measured a number density of $N_e = 10^{10}\,\mathrm{m}^{-3}$ for each 1-minute integrated altitude profile. Additionally, to meet this criteria, the associated error had to be less than $5 \times 10^9\,\mathrm{m}^{-3}$. We chose these values somewhat arbitrarily given that they are round numbers near the detection limit of PFISR. However, we did test the sensitivity and found them to be acceptably insensitive. Future, more sensitive instruments could use a smaller density threshold and thus detect lower altitudes. Finally, we implemented an outlier-rejection algorithm to remove high power returns that are not consistent with the expected electron density profile from precipitation. The D-region data can be cluttered by range-aliased satellite echoes, airplanes in antenna sidelobes, and various types of interference. Most of these clutter sources appear as localized outliers in the power data confined to one or two range-gates. We expect a realistic electron density profile to extend over 10s of km in altitude and be monotonically decreasing with altitude. We compute the median electron density over 5 km around a data point and check that it is less than the median electron density 20 km above that point. Furthermore, we check if there are any NaN or negative electron density estimates in the 20 km above that point.

3.1 Magnetic Local Time

Figure 2 panel A shows the altitude boundary values compared to MLT as calculated from the IGRF model for 2020. As we would expect, a majority of the measurements occurred several hours after magnetic midnight. Previous studies have shown that this is the most common time for pulsating aurora (Oguti et al., 1981; Jones et al., 2011). However, our data is biased towards common pulsating aurora times, as this is when we requested runs. The hourly averages shown by the black diamonds centered on each hour indicate that there may be a dip between 2 to 4 MLT, similar to previous results (Hosokawa & Ogawa, 2015; Partamies et al., 2017; E. C. Bland et al., 2019; Nanjo et al., 2021). However, due to the wide scatter of data and limited statistics for several time bins, it's difficult to say how significant this behavior is in our data.

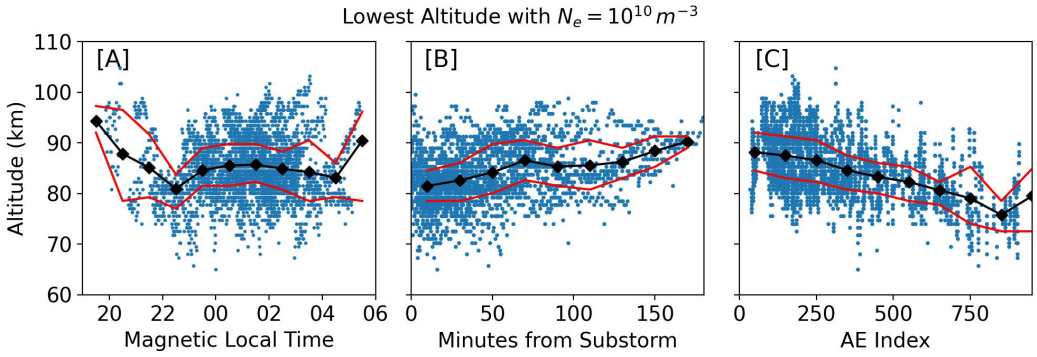

Figure 2. Lowest altitude PFISR measurements during pulsating aurora with $N_e = 10^{10}\,\mathrm{m}^{-3}$ plotted versus magnetic local time [A], time from the nearest substorm onset [B], and AE index [C]. The black diamonds indicate the average altitude for the surrounding hour, 20 minutes, 200 AE units respectively. The red lines indicate the 25% and 75% quartiles.

3.2 Substorm Proximity and AE index

Figure 2 panel B shows the altitude boundary values compared to temporal substorm proximity. Here we see that lower altitudes are more common closer to the start of a substorm, indicating a hardening of the spectrum.

Figure 2 panel C shows the altitude boundary values compared to AE index. Similar to substorm proximity, there is a clear relation between a higher AE value and lower altitudes. This matches well with Hosokawa and Ogawa (2015) who found that the peak height of pulsating aurora lowers during higher AE indices. However, our data may be more representative of the higher energy side of the spectrum since we used a lower boundary value.

We combined Figures 2B and 2C to produce Figure 3. Here we have colored the markers of Figure 2 panel B based on AE index. This result shows that both temporal substorm proximity and AE index play a role in varying the lower altitude boundary. The lowest altitudes tend to occur with both a high AE index and close temporal proximity to a substorm.

We also performed a similar analysis using AL indices, but the results did not differ in any meaningful way. A more negative AL index corresponded to lower altitudes.

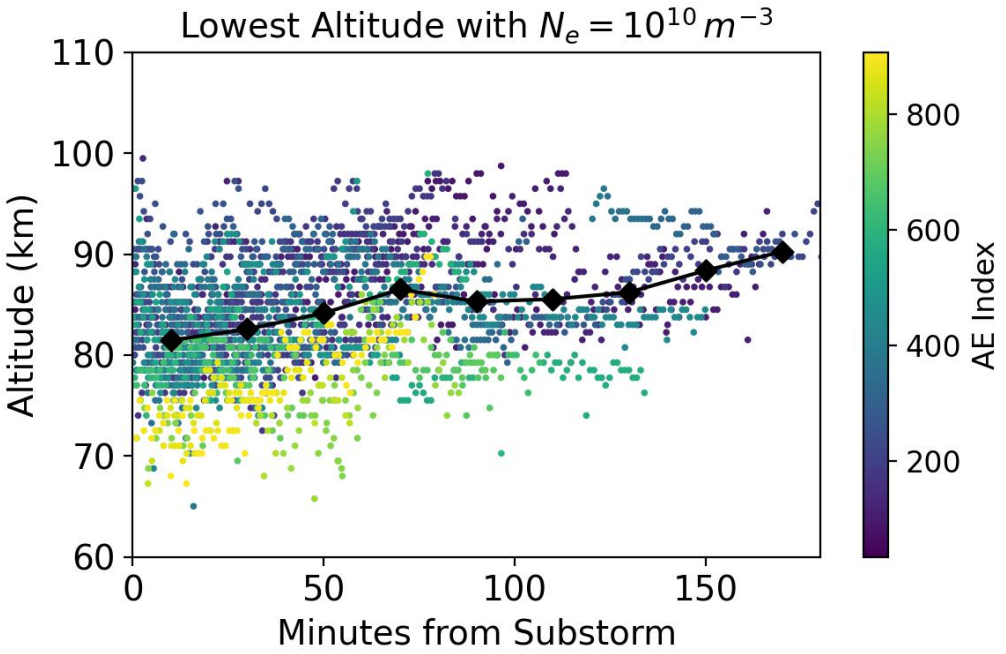

Figure 3. Lowest altitude PFISR measurements during pulsating aurora with $N_e = 10^{10}\,\mathrm{m}^{-3}$ plotted versus time from the nearest substorm onset. The markers are colored based on AE index. The black diamonds indicate the average altitude for the surrounding 20 minutes.

3.3 Energy Spectra from Electron Density Inversion

Our analysis of the lower altitude boundary with $N_e = 10^{10}\,\mathrm{m}^{-3}$ indicates that both AE index and temporal substorm proximity have significant impacts on how hard the pulsating aurora differential energy flux can be. However, this metric is only a proxy for energy. To investigate further, we solved the inverted problem required to convert the PFISR electron densities into a differential energy flux. To do this, we used the process outlined in Semeter and Kamalabadi (2005). In doing so, we assumed that the pitch angle distribution was isotropic (Whalen et al., 1971; Sandahl et al., 1980), and that the electron density varies slowly compared to the 1-minute PFISR integration time scales. We describe our exact implementation of the inversion process in supplementary Appendix 1. In an analysis like this, there are multiple spectra that could result in a reasonably good fit of the density profile, making the problem ill-defined. To help mitigate this, we chose the solution that maximized the Berg Entropy. As Semeter and Kamalabadi (2005) states, this solution "may be viewed as the most noncommittal approach with respect to the unavailable information." To further reduce uncertainty, we chose an energy threshold of 30 keV to separate the low and high portions of the differential energy flux and integrated the two regions. This gives us an average low and high energy flux and limits the dependency of our results on the specific spectral shape.

The largest source of error in the inversion process is likely the assumed atmospheric chemistry that connects PFISR observations to an ionization rate. This is not well known, especially for the D-region. As our primary chemistry model we used the Glukhov-Pasko-Inan (GPI) model (Glukhov et al., 1992; Lehtinen & Inan, 2007). This has been shown to perform well for the D-region (Marshall et al., 2019). For the E-region, we set the values above 90 km to those calculated by Gledhill (1986) for nighttime aurora. The Gledhill model is suitably close that of Vickrey et al. (1982) above 90 km and the Vickrey model has been shown to perform well in this region (Sivadas et al., 2017). While we could have used the Vickrey model, we believe the Gledhill model is slightly better for this data. However, both models are only rough estimates. We refer to this adjusted model as GPI+. To provide context to our results calculated using GPI+, we inverted each density profile using three additional chemistry models. These results can be found in supplementary Appendix 1.

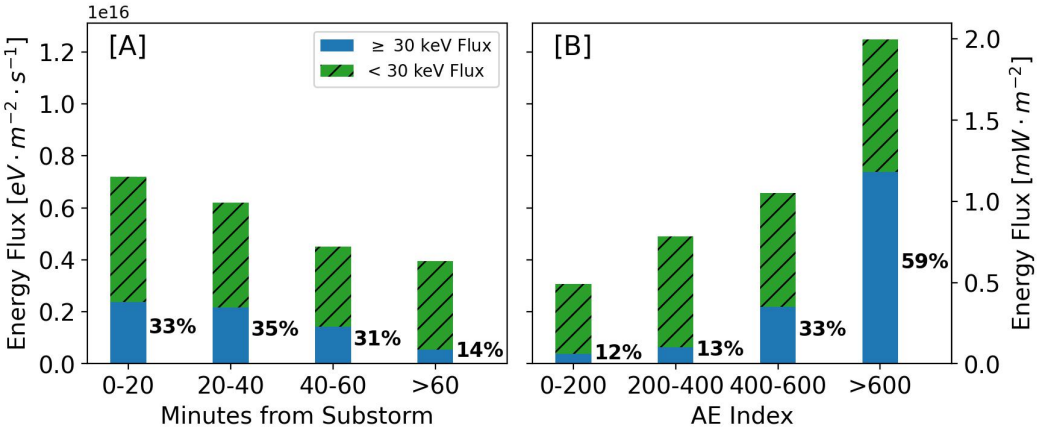

Figure 4. The high ($\geq$ 30 keV) and low ($<$ 30 keV) energy flux contributions to pulsating aurora events occurring in four temporal bins relative to substorm onset [A] and AE index [B].

After performing the inversions, we found the geometric mean for $\geq$ 30 keV and $<$ 30 keV electrons in bins relative to substorm onset and AE index. Figure 4 shows the results. While not shown here, we found similar relative behavior in analyses for energy thresholds of 50 keV and 100 keV. For $<$ 20 min the high energy contributions were 13.9% and 1.2% respectively. For $>$ 600 AE these were 37.8% and 2.4% respectively.

4 Discussion

Figure 4 summarizes our results and demonstrates the link between energy and substorm activity. This figure shows how the energy composition of pulsating aurora varies with respect to both substorm proximity [A] and AE index [B]. Within an hour of a substorm around a third of the total energy flux is carried by $\geq$ 30 keV electrons. At $>$ 60 minutes this drops to around a sixth. Interestingly, while the total energy flux climbs closer to the substorm, the energy composition remains similar all the way out to an hour after onset. This indicates that the initial substorm "kick" hardens the differential energy flux and it remains hard up to an hour afterwards, even as the total energy flux decreases.

The differential energy flux associated with AE index varies even more dramatically. In highly perturbed times of AE $>$ 600 over a half of the average energy flux is carried by the $\geq$ 30 keV electrons. This again drops to just over a tenth for quiet pe-

riods of AE $\leq$ 200. We also looked at the differential energy flux relative to AL indices, but found no difference to AE beyond a few percent.

Assumptions about the atmospheric chemistry can vary these values, but for every model we found the same relative behavior. The relative behavior was also the same when we used threshold values of 50 keV and 100 keV. Thus, we speculate with a high level of confidence that pulsating auroral energies are varied by both the strength of a substorm as well as temporal proximity to it.

The results shown in Figure 4 are significant. They clearly indicate that the energy of pulsating aurora is highly variable and that the most energetic events can have large contributions from $\geq$ 30 keV electrons. They also demonstrate that substorm timing and strength is strongly correlated with pulsating aurora energies. This suggests a process connecting substorms and pulsating aurora. There is a well documented relation between substorm activity post-midnight and whistler-mode wave generation near the equator (Tsurutani & Smith, 1974; Thorne et al., 1974). The proposed mechanism connecting them is Doppler-shifted cyclotron resonance with 10-100 keV substorm injected electrons (Dungey, 1963; Kennel & Petschek, 1966). In addition, the amplitude of already present whistler-mode waves can vary with substorm injection. Meredith et al. (2000) showed that between $3.8 < L < 6$ whistler-mode amplitudes increased after a substorm and then decayed with a timescale of $\tau \approx 1.1$ hours. That value is similar to the timescale over which we see a decrease in the spectral hardness. Given that whistler-mode waves are known to drive pulsating aurora, this is one likely explanation. Additionally, the MLT dependence of substorm driven whistler-mode waves could explain the slight increase in energetic pulsating aurora events we see post-midnight (Tsurutani & Smith, 1977).

Our results also confirm, as previous studies have hinted at, that the energetic nature of pulsating aurora is inherent to the phenomenon and not just a result of a few extreme events. This is important because pulsating aurora are very common (Oguti et al., 1981) and can be long-lasting (Jones et al., 2013). Thus they represent a relatively large transfer of energy between the magnetosphere and lower ionosphere. When considering the effects of this transfer, the total energy flux is clearly important, but so too is the hardness of the differential energy flux. Higher energy electrons reach further into the atmosphere and thus have a higher probability of influencing terrestrial climate through

processes like NO_x based ozone depletion (Turunen et al., 2016; Verronen et al., 2021, & and references therein). We found that the hardest events occur close in time to a substorm and for high AE indices. In short, our results can be used to more accurately parameterize the atmospheric consequences of pulsating aurora.

Combining the results of Figure 4 with those of E. Bland et al. (2021), we can perform a back-of-the-envelope calculation to estimate the incoming power of a typical pulsating aurora event. We will assume an event extending between 62° and 70° magnetic latitude and 4 hours of magnetic local time. Using this, approximately 4.8 gigawatts (GW) of power would be entering the atmosphere during periods with AE > 600 with 2.8 GW coming from ≥ 30 keV electrons. For periods < 20 minutes after substorm onset and all AE indices these values are 2.5 GW and 0.8 GW respectively.

It is also worth mentioning possible sources of systematic error in our results. One, several previous studies found that the electron density and differential energy flux shifts towards higher energies during the on phase of pulsating aurora (Hosokawa & Ogawa, 2015; Whalen et al., 1971). Our data is integrated over one minute, so these variations will likely be smoothed out, thus reducing the hardness. Two, we are not capturing the full range of the energy flux. Ionization associated with electron energies less than about 1 keV, usually peaks above the altitudes that PFISR measures in the D-region mode (Fang et al., 2010). If the energy flux for this portion of the spectrum is significant, we could be overestimating the spectral hardness and underestimating the total energy. Three, the sensitivity of PFISR limits our ability to detect higher energy, lower flux particles. If populations such as these are present, we could be underestimating the spectral hardness. Four, we only selected pulsating aurora that were in the center of the imager, but we didn't account for times that the PFISR beam wasn't directly on a pulsating patch. If the precipitating flux is highly local, we could be underestimating the energy flux during such periods.

5 Summary

In the field of pulsating aurora, it has been suspected that substorm activity is linked to variations in the differential energy flux of the incoming electrons. These suspicions have arisen from studies investigating proxies for energy, such as the altitude of the peak electron density. In this paper, we presented statistical evidence, using inverted energies,

that this hypothesis is correct. When pulsating aurora occurs soon after a substorm onset it is more likely to have a larger energy flux and a harder differential energy flux. This same behaviour also occurs for higher AE indices.

- The energy flux of pulsating aurora correlates strong with the temporal substorm proximity and AE index.
- In relation to temporal substorm proximity the total energy flux varies between 1.15 and 0.63 $\mathrm{mW \cdot m^{-2}}$ for $\leq$ 20 and $>$ 60 minutes. The associated contribution to the total energy flux from $\geq$ 30 keV electrons are 33% and 14%.
- In relation to substorms, the differential energy flux remains hard out to 1 hour after onset before softening.
- In relation to AE index the total energy flux varies between 2.00 and 0.49 $\mathrm{mW \cdot m^{-2}}$ for $>$ 600 and $\leq$ 200 AE indices. The associated contributions to the total energy flux from $\geq$ 30 keV electrons are 59% and 12%.
- We estimate that for a typically pulsating auroral event occurring $<$ 20 min after substorm onset (AE $>$ 600), approximately 2.5 (4.8) GW of power enters the atmosphere. The contributions from $\geq$ 30 keV electrons are 0.8 (2.8) GW.

Acknowledgments

We acknowledge the help and advice of Robert Marshall, Nithin Sivadas, and Pekka Verronen in developing our inversion analysis.

We acknowledge the substorm timing list identified by the SOPHIE technique (Forsyth et al., 2015), the Newell and Gjerloev technique (Newell & Gjerloev, 2011), the Ohtani and Gjerloev technique (Ohtani & Gjerloev, 2020), the SMU and SML indices (Newell & Gjerloev, 2011); and the SuperMAG collaboration (Gjerloev, 2012).

This material is based upon work supported by the Poker Flat Incoherent Scatter Radar, which is a major facility funded by the National Science Foundation through cooperative agreement AGS-1840962 to SRI International.

RNT was supported by the NASA FINESST award 80NSSC20K1514 to the University of Iowa.

ANJ was supported by NSF CAREER grant 2045016 to the University of Iowa.

SRK was supported by Air Force Office of Scientific Research grant FA9550-19-1-0130 to Clemson University.

References

Bland, E., Tesema, F., & Partamies, N. (2021, February). D-region impact area of energetic electron precipitation during pulsating aurora. *Annales Geophysicae*, *39*(1), 135-149. doi: 10.5194/angeo-39-135-2021

Bland, E. C., Partamies, N., Heino, E., Yukimatu, A. S., & Miyaoka, H. (2019, July). Energetic Electron Precipitation Occurrence Rates Determined Using the Syowa East SuperDARN Radar. *Journal of Geophysical Research (Space Physics)*, *124*(7), 6253-6265. doi: 10.1029/2018JA026437

Davis, T. N. (1978, January). Observed microstructure of auroral forms. *Journal of Geomagnetism and Geoelectricity*, *30*(4), 371-380. doi: 10.5636/jgg.30.371

Dungey, J. W. (1963, June). Loss of Van Allen electrons due to whistlers. *Planetary and Space Science*, *11*(6), 591-595. doi: 10.1016/0032-0633(63)90166-1

Fang, X., Randall, C. E., Lummerzheim, D., Wang, W., Lu, G., Solomon, S. C., & Frahm, R. A. (2010, November). Parameterization of monoenergetic electron impact ionization. *Geophysical Research Letters*, *37*(22), L22106. doi: 10.1029/2010GL045406

Forsyth, C., Rae, I. J., Coxon, J. C., Freeman, M. P., Jackman, C. M., Gjerloev, J., & Fazakerley, A. N. (2015, December). A new technique for determining Substorm Onsets and Phases from Indices of the Electrojet (SOPHIE). *Journal of Geophysical Research (Space Physics)*, *120*(12), 10,592-10,606. doi: 10.1002/2015JA021343

Gjerloev, J. W. (2012, September). The SuperMAG data processing technique. *Journal of Geophysical Research (Space Physics)*, *117*(A9), A09213. doi: 10.1029/2012JA017683

Gledhill, J. A. (1986, June). The effective recombination coefficient of electrons in the ionosphere between 50 and 150 km. *Radio Science*, *21*(3), 399-408. doi: 10.1029/RS021i003p00399

Glukhov, V. S., Pasko, V. P., & Inan, U. S. (1992, November). Relaxation of transient lower ionospheric disturbances caused by lightning-whistler-induced electron precipitation bursts. *Journal of Geophysical Research*, *97*(A11),

16971-16979. doi: 10.1029/92JA01596

Grono, E., & Donovan, E. (2018, June). Differentiating diffuse auroras based on phenomenology. *Annales Geophysicae*, *36*(3), 891-898. doi: 10.5194/angeo-36-891-2018

Hosokawa, K., Miyoshi, Y., Ozaki, M., Oyama, S. I., Ogawa, Y., Kurita, S., ... Fujii, R. (2020, February). Multiple time-scale beats in aurora: precise orchestration via magnetospheric chorus waves. *Scientific Reports*, *10*, 3380. doi: 10.1038/s41598-020-59642-8

Hosokawa, K., & Ogawa, Y. (2015, July). Ionospheric variation during pulsating aurora. *Journal of Geophysical Research (Space Physics)*, *120*(7), 5943-5957. doi: 10.1002/2015JA021401

Jaynes, A. N., Lessard, M. R., Rodriguez, J. V., Donovan, E., Loto'Aniu, T. M., & Rychert, K. (2013, August). Pulsating auroral electron flux modulations in the equatorial magnetosphere. *Journal of Geophysical Research (Space Physics)*, *118*(8), 4884-4894. doi: 10.1002/jgra.50434

Johnstone, A. D. (1978, July). Pulsating aurora. *Nature*, *274*(5667), 119-126. doi: 10.1038/274119a0

Jones, S. L., Lessard, M. R., Fernandes, P. A., Lummerzheim, D., Semeter, J. L., Heinselman, C. J., ... Asamura, K. (2009, May). PFISR and ROPA observations of pulsating aurora. *Journal of Atmospheric and Solar-Terrestrial Physics*, *71*(6-7), 708-716. doi: 10.1016/j.jastp.2008.10.004

Jones, S. L., Lessard, M. R., Rychert, K., Spanswick, E., & Donovan, E. (2011, March). Large-scale aspects and temporal evolution of pulsating aurora. *Journal of Geophysical Research (Space Physics)*, *116*(A3), A03214. doi: 10.1029/2010JA015840

Jones, S. L., Lessard, M. R., Rychert, K., Spanswick, E., Donovan, E., & Jaynes, A. N. (2013, June). Persistent, widespread pulsating aurora: A case study. *Journal of Geophysical Research (Space Physics)*, *118*(6), 2998-3006. doi: 10.1002/jgra.50301

Kaeppler, S. R., Sanchez, E., Varney, R. H., Irvin, R. J., Marshall, R. A., Bortnik, J., ... Reyes, P. M. (2020). Chapter 6 - incoherent scatter radar observations of 10–100kev precipitation: review and outlook. In A. N. Jaynes & M. E. Usanova (Eds.), *The dynamic loss of earth's radiation belts* (p. 145-

197). Elsevier. Retrieved from https://www.sciencedirect.com/science/article/pii/B9780128133712000068 doi: https://doi.org/10.1016/B978-0-12-813371-2.00006-8

Kasahara, S., Miyoshi, Y., Yokota, S., Mitani, T., Kasahara, Y., Matsuda, S., ... Shinohara, I. (2018, February). Pulsating aurora from electron scattering by chorus waves. *Nature*, *554*(7692), 337-340. doi: 10.1038/nature25505

Kasting, J. F., & Hays, P. B. (1977, August). A comparison between N_2 $^+$ 4278-Å emission and electron flux in the auroral zone. *Journal of Geophysical Research*, *82*(22), 3319. doi: 10.1029/JA082i022p03319

Kennel, C. F., & Petschek, H. E. (1966, January). Limit on Stably Trapped Particle Fluxes. *Journal of Geophysical Research (Space Physics)*, *71*, 1. doi: 10.1029/JZ071i001p00001

Lehtinen, N. G., & Inan, U. S. (2007, April). Possible persistent ionization caused by giant blue jets. *Geophysical Review Letters*, *34*(8), L08804. doi: 10.1029/2006GL029051

Lessard, M. R. (2012). A review of pulsating aurora. In *Auroral phenomenology and magnetospheric processes earth and other planets* (Vol. 197, pp. 5673–68). Washington, D.C. :: American Geophysical Union.

Luo, B., Li, X., Temerin, M., & Liu, S. (2013, December). Prediction of the AU, AL, and AE indices using solar wind parameters. *Journal of Geophysical Research (Space Physics)*, *118*(12), 7683-7694. doi: 10.1002/2013JA019188

Marshall, R. A., Xu, W., Kero, A., Kabirzadeh, R., & Sanchez, E. (2019, February). Atmospheric effects of a relativistic electron beam injected from above: chemistry, electrodynamics, and radio scattering. *Frontiers in Astronomy and Space Sciences*, *6*, 6. doi: 10.3389/fspas.2019.00006

Meredith, N. P., Horne, R. B., Johnstone, A. D., & Anderson, R. R. (2000, June). The temporal evolution of electron distributions and associated wave activity following substorm injections in the inner magnetosphere. *Journal of Geophysical Research*, *105*(A6), 12907-12918. doi: 10.1029/2000JA900010

Nanjo, S., Hozumi, Y., Hosokawa, K., Kataoka, R., Miyoshi, Y., Oyama, S.-i., ... Kurita, S. (2021, October). Periodicities and Colors of Pulsating Auroras: DSLR Camera Observations From the International Space Station. *Journal of Geophysical Research (Space Physics)*, *126*(10), e29564. doi:

10.1029/2021JA029564

Newell, P. T., & Gjerloev, J. W. (2011, December). Substorm and magnetosphere characteristic scales inferred from the SuperMAG auroral electrojet indices. *Journal of Geophysical Research (Space Physics)*, *116*(A12), A12232. doi: 10.1029/2011JA016936

Nishimura, Y., Bortnik, J., Li, W., Thorne, R. M., Chen, L., Lyons, L. R., ... Auster, U. (2011, November). Multievent study of the correlation between pulsating aurora and whistler mode chorus emissions. *Journal of Geophysical Research (Space Physics)*, *116*(A11), A11221. doi: 10.1029/2011JA016876

Nishimura, Y., Bortnik, J., Li, W., Thorne, R. M., Lyons, L. R., Angelopoulos, V., ... Auster, U. (2010, October). Identifying the Driver of Pulsating Aurora. *Science*, *330*(6000), 81. doi: 10.1126/science.1193186

Oguti, T., Kokubun, S., Hayashi, K., Tsuruda, K., Machida, S., Kitamura, T., ... Watanabe, T. (1981, August). Statistics of pulsating auroras on the basis of all-sky TV data from five stations. I. Occurrence frequency. *Canadian Journal of Physics*, *59*, 1150-1157. doi: 10.1139/p81-152

Ohtani, S., & Gjerloev, J. W. (2020, September). Is the Substorm Current Wedge an Ensemble of Wedgelets?: Revisit to Midlatitude Positive Bays. *Journal of Geophysical Research (Space Physics)*, *125*(9), e27902. doi: 10.1029/2020JA027902

Oyama, S., Kero, A., Rodger, C. J., Clilverd, M. A., Miyoshi, Y., Partamies, N., ... Saito, S. (2017, June). Energetic electron precipitation and auroral morphology at the substorm recovery phase. *Journal of Geophysical Research (Space Physics)*, *122*(6), 6508-6527. doi: 10.1002/2016JA023484

Partamies, N., Whiter, D., Kadokura, A., Kauristie, K., Nesse Tyssøy, H., Massetti, S., ... Raita, T. (2017, May). Occurrence and average behavior of pulsating aurora. *Journal of Geophysical Research (Space Physics)*, *122*(5), 5606-5618. doi: 10.1002/2017JA024039

Royrvik, O., & Davis, T. N. (1977, October). Pulsating aurora: Local and global morphology. *Journal of Geophysical Research*, *82*(29), 4720. doi: 10.1029/JA082i029p04720

Sandahl, I., Eliasson, L., & Lundin, R. (1980, May). Rocket observations of precipitating electrons over a pulsating aurora. *Geophysical Research Letters*, *7*(5),

309-312. doi: 10.1029/GL007i005p00309

Semeter, J., & Kamalabadi, F. (2005, April). Determination of primary electron spectra from incoherent scatter radar measurements of the auroral E region. *Radio Science*, *40*(2), RS2006. doi: 10.1029/2004RS003042

Sivadas, N., Semeter, J., Nishimura, Y., & Kero, A. (2017, October). Simultaneous Measurements of Substorm-Related Electron Energization in the Ionosphere and the Plasma Sheet. *Journal of Geophysical Research (Space Physics)*, *122*(10), 10,528-10,547. doi: 10.1002/2017JA023995

Thorne, R. M., Smith, E. J., Fiske, K. J., & Church, S. R. (1974, January). Intensity variation of ELF hiss and chorus during isolated substorms. *Geophysical Research Letters*, *1*(5), 193-196. doi: 10.1029/GL001i005p00193

Tsurutani, B. T., & Smith, E. J. (1974, January). Postmidnight chorus: A substorm phenomenon. *Journal of Geophysical Research (Space Physics)*, *79*(1), 118-127. doi: 10.1029/JA079i001p00118

Tsurutani, B. T., & Smith, E. J. (1977, November). Two types of magnetospheric ELF chorus and their substorm dependences. *Journal of Geophysical Research*, *82*(32), 5112. doi: 10.1029/JA082i032p05112

Turunen, E., Kero, A., Verronen, P. T., Miyoshi, Y., Oyama, S.-I., & Saito, S. (2016, October). Mesospheric ozone destruction by high-energy electron precipitation associated with pulsating aurora. *Journal of Geophysical Research (Atmospheres)*, *121*(19), 11,852-11,861. doi: 10.1002/2016JD025015

Verronen, P. T., Kero, A., Partamies, N., Szelag, M. E., Oyama, S.-I., Miyoshi, Y., & Turunen, E. (2021, October). Simulated seasonal impact on middle atmospheric ozone from high-energy electron precipitation related to pulsating aurorae. *Annales Geophysicae*, *39*(5), 883-897. doi: 10.5194/angeo-39-883-2021

Vickrey, J. F., Vondrak, R. R., & Matthews, S. J. (1982, July). Energy deposition by precipitating particles and Joule dissipation in the auroral ionosphere. *Journal of Geophysical Research*, *87*(A7), 5184-5196. doi: 10.1029/JA087iA07p05184

Whalen, B. A., Miller, J. R., & McDiarmid, I. B. (1971, January). Energetic particle measurements in a pulsating aurora. *Journal of Geophysical Research*, *76*(4), 978. doi: 10.1029/JA076i004p00978

Wing, S., Gkioulidou, M., Johnson, J. R., Newell, P. T., & Wang, C.-P. (2013,

493 March). Auroral particle precipitation characterized by the substorm cycle.
494 *Journal of Geophysical Research (Space Physics)*, *118*(3), 1022-1039. doi:
495 10.1002/jgra.50160